Fast evaluation of zero-offset Green's function for layered media with application to ground-penetrating radar

Sébastien Lambot,[1,2] Evert Slob,[3] and Harry Vereecken[2]

Received 31 July 2007; revised 24 September 2007; accepted 12 October 2007; published 14 November 2007.

[1] We propose an efficient integration path for the fast evaluation of the three-dimensional spatial-domain Green's function for electromagnetic wave propagation in layered media for the particular case of zero-offset, source-receiver proximal ground-penetrating radar (GPR) applications. The integration path is deformed in the complex plane of the integration variable k_ρ so that the oscillations of the dominant exponential term in the spectral Green's function are minimized. The contour does not need to be closed back on the real k_ρ axis as the complex integrand rapidly damps. The accuracy and efficiency of the technique have been confirmed by comparison with traditional elliptic integration contours. The proposed algorithm appears to be promising development for fast, full-wave modeling and inversion of GPR data. **Citation:** Lambot, S., E. Slob, and H. Vereecken (2007), Fast evaluation of zero-offset Green's function for layered media with application to ground-penetrating radar, *Geophys. Res. Lett.*, *34*, L21405, doi:10.1029/2007GL031459.

1. Introduction

[2] Modeling electromagnetic wave propagation in three-dimensional (3-D) layered media is essential in many application areas such as geophysical prospecting, remote sensing, monolithic integrated circuits, or microstrip antennas. In particular, it is increasingly used for modeling ground-penetrating radar (GPR) wave propagation in the subsurface [*Spagnolini*, 1997; *Gentili and Spagnolini*, 2000; *Lambot et al.*, 2004]. The work on layered media must be ascribed to Sommerfeld who, as early as 1909, analyzed radiowave propagation above lossy ground [*Sommerfeld*, 1909]. Solving Maxwell's equations for layered media is now well known [*Chew*, 1990; *Michalski and Mosig*, 1997] and entails the concept of Green's function, defined as the fields created by a unit point source embedded in the layered medium. Given the invariance of the electromagnetic properties along the two horizontal coordinate directions, closed form expressions for the Green's functions can be found in the spectral domain. The corresponding spatial domain Green's functions are subsequently obtained through Sommerfeld-type integrals over an unbounded interval. These integrals usually constitute a critical point, as the integrand is characterized by the presence of singularities, i.e., surface wave poles and branch points, and has a highly oscillating behavior resulting in slow integration convergence [*Aksun and Dural*, 2005].

[3] Extensive research has been devoted to the evaluation of these integrals through methods such as singularity extraction techniques [*Simsek et al.*, 2006; *Polimeridis et al.*, 2007], the fast Hankel transform [*Hanson*, 2004; *Boix et al.*, 2007], the steepest descent path [*Cui and Chew*, 1999; *Tsang et al.*, 2006], the discrete complex image method [*Chow et al.*, 1991; *Aksun and Mittra*, 1992; *Yuan et al.*, 2006; *Zhuang et al.*, 2007], and acceleration techniques for unbounded integration of oscillating functions [*Michalski*, 1998]. In particular, the poles and branch points can be avoided by deforming the integration path in the complex k_ρ plane using, for example, rectangular or elliptic contours, and by applying Cauchy's integral theorem [*GayBalmaz and Mosig*, 1997; *Paulus et al.*, 2000; *He et al.*, 2005; *Simsek et al.*, 2006]. However, while all these techniques have proven to be accurate and efficient, they are usually valid only for particular layered configurations or source-receiver relative positions. The definition of the integration contours often remains partly subjective. For instance, *Paulus et al.* [2000] and *Simsek et al.* [2006] considered an empirical ratio of 10^{-3} between the semi-minor and semi-major axes of an elliptic integration path, leaving the contour in relatively close vicinity to the real axis in order to avoid significant increase in the Bessels functions.

[4] In relation to the off-ground monostatic GPR modeling approach proposed by *Lambot et al.* [2004], we analyze the spectral Green's function behavior for the particular case of zero-offset source-receiver configuration for wave propagation in general layered media. An optimal integration path is proposed in order to evaluate the spatial domain Green's function accurately and efficiently. Such a procedure is particularly advantageous when performing full-wave inverse modeling of radar data, which requires a large number of forward runs, or when dealing with continuously varying electromagnetic media, for which the computation of the Green's function is relatively time-consuming. Indeed, such media are usually emulated using a large number of layers that are thin enough to be a minor fraction of the minimal wavelength [*Lambot et al.*, 2006].

2. Zero-Offset Green's Function

[5] A general formulation of spatial-domain Green's function $G(\rho)$ in terms of Sommerfeld integral S_n for wave propagation in layered media can be expressed as:

$$G(\rho) = S_n\left[\tilde{G}\right] = \int_0^{+\infty} J_n\left(k_\rho \rho\right)\tilde{G}\left(k_\rho\right)k_\rho^{n+1}dk_\rho \qquad (1)$$

[1]Department of Environmental Sciences and Land Use Planning, Université Catholique de Louvain, Louvain-la-Neuve, Belgium.
[2]ICG-4 Agrosphere, Institute of Chemistry and Dynamics of the Geosphere, Forschungszentrum Jülich GmbH, Jülich, Germany.
[3]Department of Geotechnology, Delft University of Technology, Delft, Netherlands.

0094-8276/07/2007GL031459$05.00

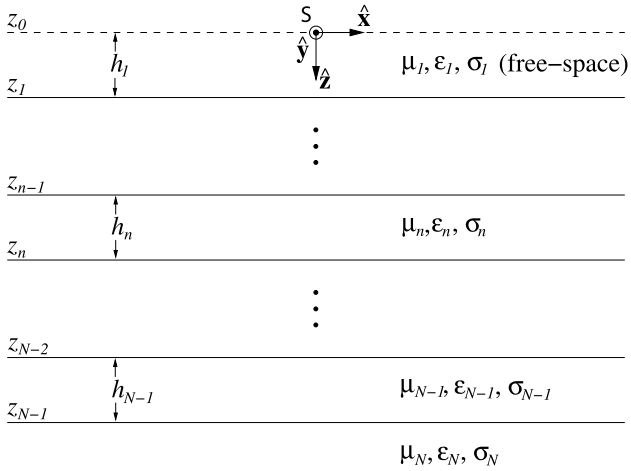

Figure 1. Three-dimensional N-layered medium with a point source-receiver at the origin $\mathcal{S}$ of the coordinate system. The medium of the nth layer is characterized by constant magnetic permeability (μ_n), dielectric permittivity ε_n, electric conductivity σ_n, and thickness h_n.

where J_n is the Bessel function of order n, $\tilde{G}(k_\rho)$ is a generic spectral Green's function, ρ is the distance between the source and the receiver, and k_ρ is its spectral domain counterpart.

[6] In the model configuration considered here, depicted in Figure 1, the source and the receiver are both situated at the same point in free-space at some distance above the layered medium interfaces. This describes the radar antenna configuration above the soil surface. The Green's function is defined as the x-directed component of the reflected electric field for a unit-strength x-directed electric current source [*Lambot et al.*, 2004]. The incident field is, therefore, subtracted from the total field to avoid the singularity at the source where the total field tends to infinity. As the distance ρ between the source and the receiver is zero, the Bessel's functions vanish in the Sommerfeld integral, resulting in an ordinary infinite integral. The spatial Green's function at the source point reduces to:

$$G = \int_0^{+\infty} \underbrace{\tilde{G}(k_\rho) k_\rho}_{I} \, dk_\rho \tag{2}$$

where the spectral Green's function is found to be:

$$\tilde{G}(k_\rho) = \underbrace{\frac{1}{8\pi}\left(\frac{\Gamma_1 R_1^{TM}}{\sigma_1 + \jmath\omega\varepsilon_1} - \frac{\jmath\omega\mu_1 R_1^{TE}}{\Gamma_1}\right)}_{I_2} \underbrace{\exp(-2\Gamma_1 h_1)}_{I_1} \tag{3}$$

In this expression, the subscripts denote layer indexes, R^{TM} and R^{TE} are, respectively, the transverse magnetic (TM) and transverse electric (TE) global reflection coefficients accounting for all reflections and multiples from inferior interfaces, Γ is the vertical wavenumber defined as $\Gamma = \sqrt{k_\rho^2 - k^2}$, whilst $k^2 = \omega^2\mu(\varepsilon - \frac{\jmath\sigma}{\omega})$ with ω being the angular frequency. For the free-space layer 1, we have $k_1^2 = (\frac{\omega}{c})^2$ with c being the free-space wave velocity.

[7] The global TM-mode and TE-mode reflection coefficients at interface n are given by [*Slob and Fokkema*, 2002]:

$$R_n^{TM} = \frac{r_n^{TM} + R_{n+1}^{TM}\exp(-2\Gamma_{n+1}h_{n+1})}{1 + r_n^{TM}R_{n+1}^{TM}\exp(-2\Gamma_{n+1}h_{n+1})} \tag{4}$$

$$r_n^{TM} = \frac{(\sigma_{n+1} + \jmath\omega\varepsilon_{n+1})\Gamma_n - (\sigma_n + \jmath\omega\varepsilon_n)\Gamma_{n+1}}{(\sigma_{n+1} + \jmath\omega\varepsilon_{n+1})\Gamma_n + (\sigma_n + \jmath\omega\varepsilon_n)\Gamma_{n+1}} \tag{5}$$

$$R_n^{TE} = \frac{r_n^{TE} + R_{n+1}^{TE}\exp(-2\Gamma_{n+1}h_{n+1})}{1 + r_n^{TE}R_{n+1}^{TE}\exp(-2\Gamma_{n+1}h_{n+1})} \tag{6}$$

$$r_n^{TE} = \frac{\mu_{n+1}\Gamma_n - \mu_n\Gamma_{n+1}}{\mu_{n+1}\Gamma_n + \mu_n\Gamma_{n+1}} \tag{7}$$

where r_n^{TM} and r_n^{TE} denote the Fresnel TM and TE mode reflection coefficients at interface n ($n = 1 \cdots N-1$). R_1^{TM} and R_1^{TE} in equation (3) can be computed recursively from $n = N-1 \cdots 1$, considering that there are no upgoing waves from the lower half-space, i.e., $R_{N-1}^{TM} = r_{N-1}^{TM}$ and $R_{N-1}^{TE} = r_{N-1}^{TE}$.

[8] The spectral Green's function (3) contains various singularities originating from poles and branch points. The poles are due to vanishing denominators and correspond, physically, to modes guided by the layered medium (surface wave poles). Branch points originate from the Γ dependence and since Γ is the square root of a complex number, it is doubled valued and has branch cuts defined by $\mathrm{Im}(\Gamma) = 0$ that intersect the plane of integration. Each branch cut ends in a branch point at $k_\rho = \pm k$. If the medium is lossless, these singularities are located on the real k_ρ axis. For lossy media, they are situated in the negative imaginary k_ρ plane, as the integration runs from zero to infinity. A branch cut exists for each layer n [*Chew*, 1995].

[9] In Figure 2, we illustrate the behavior of the integrand I (equation (2)) and its major components I_1 and I_2 (equation (3)) with respect to the integration variable k_ρ along the real axis. In this example, the layered medium consists of $N = 4$ layers, including the two outermost half-spaces, with $\varepsilon_{1\ldots4} = \varepsilon_0 \cdot \{1, 9, 12, 4\}$ Fm^{-1}, $\sigma_{1\ldots4} = \{0, 0.001, 0.05, 0.1\}$ Sm^{-1}, and $h_{1\ldots4} = \{0.25, 0.30, 0.30, \infty\}$ m, with ε_0 being the free-space dielectric permittivity. The frequency is 1 GHz.

[10] For the exponential term I_1, we initially observe a strong oscillating behavior for $k_\rho < k_1$, due to its complex valued argument. At $k_\rho = k_1$, the function exhibits a branch point. For $k_\rho > k_1$, the exponential is real and decays rapidly. The component I_2 is highly oscillating for $k_\rho < \max(\mathrm{Re}(k_n))$ due to the exponential terms in the global reflection coef-

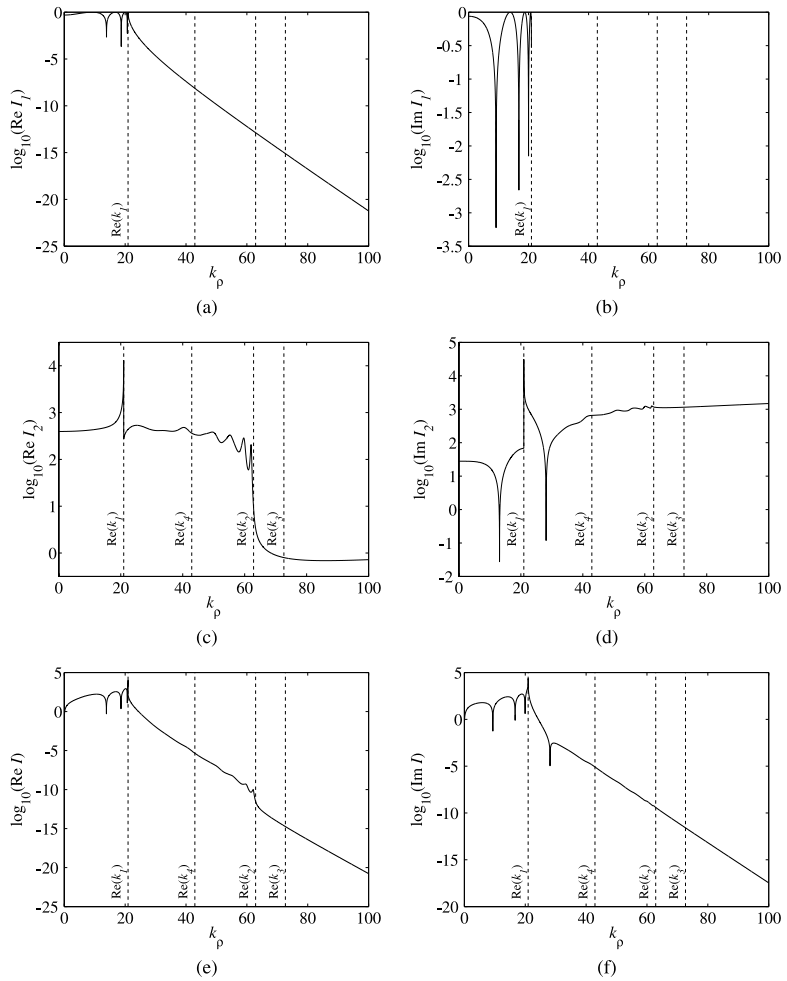

Figure 2. Real and imaginary parts of integrand components (a and b) I_1 and (c and d) I_2 and (e and f) full integrand I along the real k_ρ axis. The dashed lines correspond to the zeros of the vertical wavenumbers projected on the real axis.

ficients. A pole can be observed for $k_\rho = k_1$ and the effect of a branch point is observed for $k_\rho = k_2$ for which the electric conductivity is relatively small (the branch point is therefore close to the real k_ρ axis). In Figures 2e and 2f, the full integrand appears to be dominated essentially by the I_1 exponential, oscillating for low k_ρ values and rapidly decaying for high k_ρ values.

3. Optimal Integration Path

[11] To ensure proper and fast convergence of the integral, the integration path should avoid the integrand singularities and the function oscillations should be minimized. The poles and the branch points occurring for negative values of $\mathrm{Im}(k_\rho)$ (see definition of Γ above), it is convenient to deform the path in the positive part of the complex k_ρ plane. This avoids, in particular, the need to determine all singularities, which can be cumbersome. Given the dominating effect of I_1 in the spectral Green's function, the proposed approach is to follow the path that minimizes its oscillating behavior. This means that the imaginary part of the square root in the exponential should be constant (constant phase) and equal to its value at $k_\rho = 0$, where the integration is initiated.

[12] Defining k_ρ as the complex number $(x + jy)$ in Γ_1, and changing variables so that $a = x\frac{c}{\omega}$ and $b = y\frac{c}{\omega}$, we find:

$$\mathrm{Im}(\Gamma_1) = \mathrm{Im}\left(\sqrt{(a+jb)^2-1}\right) = \frac{1}{2}\sqrt{2+2\sqrt{a^4+2a^2b^2-2a^2+b^4+2b^2+1}-2a^2+2b^2} \tag{8}$$

For $k_\rho = 0$, we find $\mathrm{Im}(\Gamma_1) = 1$. Substituting this value in (8), we obtain the following relationship for the constant phase integration path:

$$y(x) = \frac{x}{\sqrt{\left(\frac{xc}{\omega}\right)^2+1}} \tag{9}$$

[13] Figure 3 represents the real and imaginary parts of the integrand components I_1 and I_2 and full integrand I in the complex k_ρ plane for the example above. The proposed optimal path is also represented and compared to a commonly used elliptic path closed on the real axis. We observe that the decaying exponential term I_1 strongly determines the behavior of the integrand I in the complex plane. As x

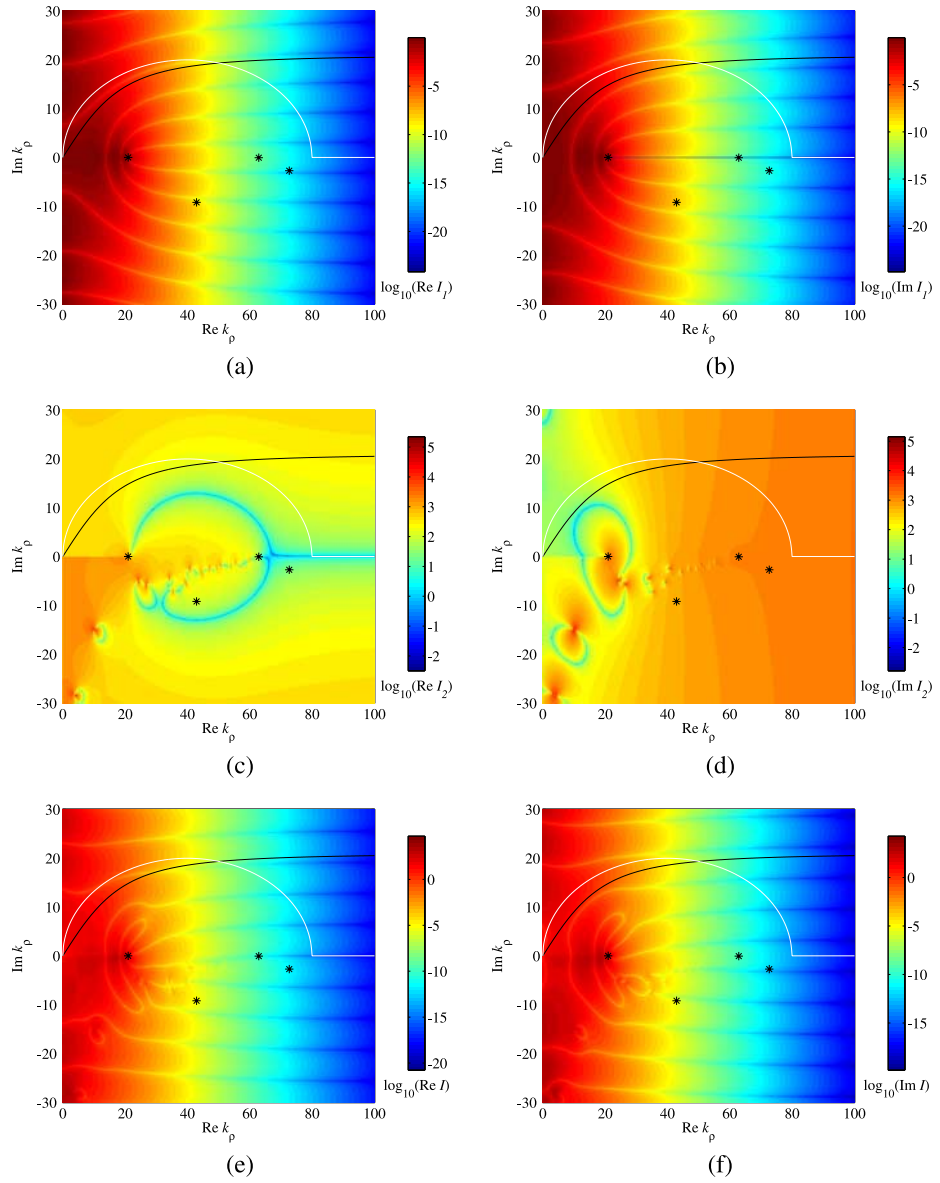

Figure 3. Real and imaginary parts of the integrand components (a and b) I_1 and (c and d) I_2 and (e and f) full integrand I in the complex k_ρ plane. The black curve represents the optimal integration path. The white curve represents an elliptic path closed on the real axis. The asterisks correspond to the zeros of the vertical wavenumbers (see also Figure 2).

increases (for $x > k_1$), the integrand I strongly decays for any y values, and particularly, following the optimal integration path as defined by (9). Therefore, closing the optimal integration path on the real axis, as required by Cauchy's integral theorem, is not necessary as the residual integrand becomes negligible for sufficiently high x values. In order to satisfy a specific accuracy for the evaluation of the integral, an upper limit $x_{\max}$ of integration can be defined. Given the negligible contribution of I_2 for large x values, the criterion can be defined using the damping factor of the exponential component I_1 only. For instance, for a damping factor of $d = 10^{-16}$ in the example above, $x_{\max}$ can be computed as:

$$x_{\max} = \sqrt{\left(\frac{-\ln d}{2h_1}\right)^2 + \left(\frac{\omega}{c}\right)^2} = 124.6 \qquad (10)$$

[14] Following these considerations, and applying Cauchy's integral theorem, the spatial domain Green's function can be computed as follows:

$$G = \int_0^{x_{\max}} \tilde{G}(x + \jmath y(x)) \cdot [x + \jmath y(x)] \frac{\partial (x + \jmath y(x))}{\partial x} dx \qquad (11)$$

with

$$\frac{\partial (x + \jmath y(x))}{\partial x} = 1 + \jmath \left(\frac{1}{\sqrt{\left(\frac{xc}{\omega}\right)^2 + 1}} - \frac{x^2}{\sqrt{\left(\left(\frac{xc}{\omega}\right)^2 + 1\right)^3}} \frac{c^2}{\omega^2} \right) \qquad (12)$$

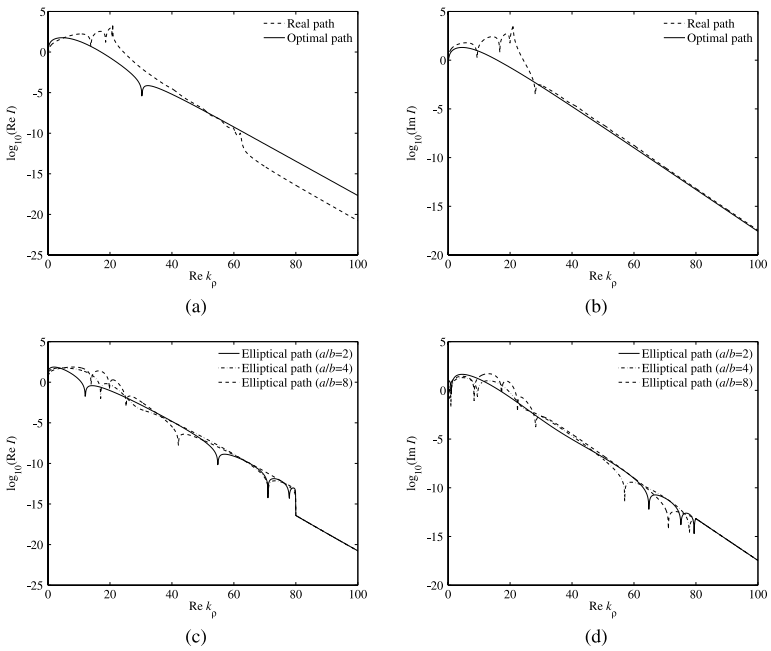

Figure 4. Real and imaginary parts of the integrand following the real k_ρ axis, the optimal path, and a series of elliptic paths with different semi-axis ratios. a is the major axis and b is the minor axis of the elliptic contour.

This proper integral can be calculated numerically by using Gaussian quadratures.

4. Results

[15] Figure 4 represents the values of the integrand following the real k_ρ axis, the optimal path (following equation (9)), and a series of elliptic paths with different semi-axis ratios. As expected, we observe that the proposed path exhibits the smallest oscillations, which is favorable for an accurate and fast integration. The asymptotic behavior of the integrand, especially its real part, is different compared to the real axis path. Yet, this difference strongly decreases due to the rapid exponential damping. The elliptic path shows various degrees of oscillations. We have compared the effect of these oscillations on the computation time for evaluating the integral (results not presented) and as expected, a faster integration was obtained for the optimal path, with a speed-up factor varying between 1.4 and 4.6, depending on the semi-ellipse. When the elliptic path follows the optimal path closely (e.g., as in Figure 3), the gain is minimal. However, such an optimal axis ratio is not known a priori in practice. The benefit becomes more significant (>4) for other axis ratios, like, e.g., 10^{-3} as adopted by *Paulus et al.* [2000] and *Simsek et al.* [2006].

5. Conclusions

[16] In this paper, an optimal integration path for evaluating the zero-offset layered media Green's function is presented. Since the integral is calculated numerically with the desired accuracy, the complete procedure is error controllable. Compared to a traditional elliptic contour, it significantly reduces the integration time, up to a factor of 5. The proposed algorithm appears to be very promising potential for the inversion of off-ground GPR data using full-wave modeling. Future work will focus on the investigation of the validity domain of the technique, particularly when the radar antenna is closer to soil surface and for other frequencies.

[17] **Acknowledgments.** This work was supported by the Forschungszentrum Jülich GmbH (Germany), Delft University of Technology (The Netherlands), FNRS (Fonds National de la Recherche Scientifique, Belgium), and Université Catholique de Louvain (Belgium).

References

Aksun, M. I., and G. Dural (2005), Clarification of issues on the closed-form Green's functions in stratified media, *IEEE Trans. Antennas Propag.*, *53*, 3644–3653.

Aksun, M. I., and R. Mittra (1992), Derivation of closed-form Green-functions for a general microstrip geometry, *IEEE Trans. Microwave Theory Tech.*, *40*(11), 2055–2062.

Boix, R. R., F. Mesa, and F. Medina (2007), Application of total least squares to the derivation of closed-form Green's functions for planar layered media, *IEEE Trans. Microwave Theory Tech.*, *55*(2), 268–280.

Chew, W. C. (1990), *Waves and Fields in Inhomogeneous Media*, Van Nostrand Reinhold, New York.

Chew, W. C. (1995), *Waves and Fields in Inhomogeneous Media*, IEEE Press, Piscataway, NJ.

Chow, Y. L., J. J. Yang, D. G. Fang, and G. E. Howard (1991), A closed-form spatial Greens-function for the thick microstrip substrate, *IEEE Trans. Microwave Theory Tech.*, *39*(3), 588–592.

Cui, T. J., and W. C. Chew (1999), Fast evaluation of Sommerfeld integrals for EM scattering and radiation by three-dimensional buried objects, *IEEE Trans. Geosci. Remote Sens.*, *37*, 887–900.

GayBalmaz, P., and J. R. Mosig (1997), Three-dimensional planar radiating structures in stratified media, *Int. J. Microwave Millimeter Wave Comput. Aided Eng.*, *7*(5), 330–343.

Gentili, G. G., and U. Spagnolini (2000), Electromagnetic inversion in monostatic ground penetrating radar: TEM horn calibration and application, *IEEE Trans. Geosci. Remote Sens.*, *38*, 1936–1946.

Hanson, G. W. (2004), Dyadic Green's function for a multilayered planar medium—A dyadic eigenfunction approach, *IEEE Trans. Antennas Propag.*, *52*, 3350–3356.

He, X. L., S. X. Gong, and Q. Z. Liu (2005), Fast computation of spatial Green's functions of multilayered microstrip antennas, *Microwave Opt. Technol. Lett.*, *45*(1), 85–88.

Lambot, S., E. C. Slob, I. van den Bosch, B. Stockbroeckx, and M. Vanclooster (2004), Modeling of ground-penetrating radar for accurate characteriza-

tion of subsurface electric properties, *IEEE Trans. Geosci. Remote Sens.*, *42*, 2555–2568.

Lambot, S., E. C. Slob, M. Vanclooster, and H. Vereecken (2006), Closed loop GPR data inversion for soil hydraulic and electric property determination, *Geophys. Res. Lett.*, *33*, L21405, doi:10.1029/2006GL027906.

Michalski, K. A. (1998), Extrapolation methods for Sommerfeld integral tails, *IEEE Trans. Antennas Propag.*, *46*, 1405–1418.

Michalski, K. A., and J. R. Mosig (1997), Multilayered media Green's functions in integral equation formulations, *IEEE Trans. Antennas Propag.*, *45*, 508–519.

Paulus, M., P. Gay-Balmaz, and O. J. F. Martin (2000), Accurate and efficient computation of the Green's tensor for stratified media, *Phys. Rev. E*, *62*, 5797–5807.

Polimeridis, A. G., T. V. Yioultsis, and T. D. Tsiboukis (2007), An efficient pole extraction technique for the computation of Green's functions in stratified media using a sine transformation, *IEEE Trans. Antennas Propag.*, *55*, 227–229.

Simsek, E., Q. H. Liu, and B. J. Wei (2006), Singularity subtraction for evaluation of Green's functions for multilayer media, *IEEE Trans. Microwave Theory Tech.*, *54*(1), 216–225.

Slob, E., and J. Fokkema (2002), Coupling effects of two electric dipoles on an interface, *Radio Sci.*, *37*(5), 1073, doi:10.1029/2001RS002529.

Sommerfeld, A. (1909), Propagation of waves in wireless telegraphy, *Ann. Phys.*, *28*, 665–736.

Spagnolini, U. (1997), Permittivity measurements of multilayered media with monostatic pulse radar, *IEEE Trans. Geosci. Remote Sens.*, *35*, 454–463.

Tsang, L., C. J. Ong, and B. P. Wu (2006), Electromagnetic fields of Hertzian dipoles in thin-layered media, *IEEE Antennas Wireless Prop. Lett.*, *5*, 537–540.

Yuan, M. T., T. K. Sarkar, and M. Salazar-Palma (2006), A direct discrete complex image method from the closed-form Green's functions in multilayered media, *IEEE Trans. Microwave Theory Tech.*, *54*(3), 1025–1032.

Zhuang, L., G. Q. Zhu, Y. H. Zhang, and B. X. Xiao (2007), An improved discrete complex image method for Green's functions in multilayered media, *Microwave Opt. Technol. Lett.*, *49*(6), 1337–1340.

S. Lambot, Department of Environmental Sciences and Land Use Planning, Université Catholique de Louvain, Croix du Sud 2 Box 2, B-1348 Louvain-la-Neuve, Belgium. (sebastien.lambot@uclouvain.be)

E. Slob, Department of Geotechnology, Delft University of Technology, Stevinweg 1, NL-2628 CN Delft, Netherlands. (e.c.slob@tudelft.nl)

H. Vereecken, ICG-4 Agrosphere, Institute of Chemistry and Dynamics of the Geosphere, Forschungszentrum Jülich GmbH, D-52425 Jülich, Germany. (s.lambot@fz-juelich.de; h.vereecken@fz-juelich.de)